PAPER

Check for updates

Accelerated oxidation of mustard gas analog with PVA-based hydrogels

Erika L. De Leon, [a] Hunter A. Anderson,[a] Daichi Maruyama,[b] Scott A. Darveau, [b] Daniel J. Van Buren,[c] Martha D. Morton [a] and Chin Li Cheung [*a]

Sulfur mustard (HD) is a hydrophobic, volatile chemical warfare agent (CWA) that has been shown to contaminate surfaces as a solid residue. This sparks an ongoing search to rid HD residue from contaminated sensitive equipment with a simple, disposable material-based solution. Hydrogels as tunable polymeric matrices fit this niche due to their potential in formulating environment-friendly remediators for CWAs. The oxidation of sulfur in HD and its analogs affords fast methods for decontamination with minimal intermediates. Here we report our study of polyvinyl-alcohol (PVA)-based hydrogels comprising a bicarbonate-activated peroxide (BAP) system (ammonium bicarbonate and hydrogen peroxide (NH_4HCO_3–H_2O_2)) to release a strong oxidizer, peroxymonocarbonate ions (HCO_4^-), for long-term HD remediation at nearly neutral pH. The production of HCO_4^- by the PVA-based hydrogels with different concentrations of H_2O_2 was verified by NMR and Raman spectroscopy. The efficacies of these hydrogels on HD remediation were evaluated using the HD simulant, 2-chloroethyl ethyl sulfide (CEES). The amine oxide surfactant, *N,N*-dimethyl-1-dodecylamine *N*-oxide (DDAO), was incorporated into these BAP-enhanced hydrogels to facilitate the oxidation of CEES by increasing its solubility in the hydrogels. Through ^{13}C-NMR analysis, a PVA-based hydrogel with BAP and DDAO was demonstrated to remediate 90% of CEES through accelerated oxidation (82%) and hydrolysis (8%) within 10 minutes. Additionally, the examination using headspace gas chromatography-mass spectrometry of the gas above a CEES-containing hydrogel showed that the relative concentration of CEES decreased by 99% within 60 to 80 minutes. Our illustrated combined use of HCO_4^- and amine oxide surfactants for boosting oxidative kinetics validates the versatility of this approach for applications with other gel-capture systems for advancing decontamination methods for hydrophobic substrates.

1 Introduction

The development of easy-to-use and disposable materials for decontaminating chemical warfare agents (CWAs) remains a critical pursuit to safeguard frontline personnel. One notable CWA is sulfur-based mustard gas (HD), which has been used since World War I.[1] HD is notorious for its lingering presence in the air and its ability to cause severe burns upon exposure.[2] Additionally, HD's hydrophobic nature allows it to adhere to surfaces, complicating its removal.[3] According to the U.S. Centers for Disease Control and Prevention, HD can remain in the air for one to two days under average weather conditions, and it has no known cure.[4] Typical environmental treatments involve chemical breakdown with hot water and/or caustic agents such as sodium hydroxide.[5] The subsequent byproducts

are further treated using oxidation or biotreatment, as recently reported by the city of Pueblo, Colorado, in the US.[6]

Developments of remediation methods for HD often utilize 2-chloroethyl ethyl sulfide (CEES) as an HD simulant. Three typical chemical pathways[7] explored in methods for destroying
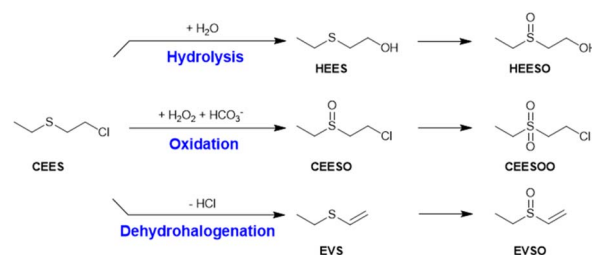

Scheme 1 Three common pathways of neutralizing 2-chloroethyl ethyl sulfide (CEES): hydrolysis, oxidation, and dehydrohalogenation. The hydrolysis pathway forms hydroxyethyl ethyl sulfide (HEES) and hydroxyethyl ethyl sulfoxide (HEESO) while the oxidation pathway forms 2-chloroethyl ethyl sulfoxide (CEESO) and 2-chloroethyl ethyl sulfonate (CEESOO). Ethyl vinyl sulfide (EVS) and ethyl vinyl sulfoxide (EVSO) are formed from the dehydrohalogenation pathway.

aDepartment of Chemistry, University of Nebraska-Lincoln, Lincoln, NE, 68588, USA. E-mail: ccheung2@unl.edu

bDepartment of Chemistry, University of Nebraska at Kearney, Kearney, NE, 68849, USA

cNational Strategic Research Institute, Omaha, NE, 68198, USA
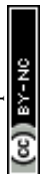
CEES are hydrolysis, oxidation, and dehydrohalogenation (Scheme 1). Among these three pathways, oxidation is the fastest, and therefore it leads to fewer intermediates.[8] Consequently, many remediation methods focus on promoting the oxidation of CEES to its less toxic product, 2-chloroethyl ethyl sulfoxide (CEESO). Most studies of decontamination methods for CEES focus on reactions in organic solutions or neat conditions[9] because CEES has low solubility in aqueous media due to its hydrophobic nature.[10] Under these organic solvents or neat conditions, catalysts such as metal oxides,[11,12] carbon materials,[13,14] zeolites,[15] and polyoxometalates[16] have been reported to promote the decomposition of CEES with destruction and removal efficiency (DRE) from 36% up to 93% in 24 hours.

A water-rich environment for oxidation has great potential to increase the scope of reactions performed on CEES and decrease the production of toxic byproducts. Performing the oxidation of CEES *via* hydrogels fits this criterion. Hydrogels are a 3D matrix of polymer chains that resist dissolution in aqueous environments and maintain functionality under physiological conditions.[17] Hydrogels containing polyvinyl alcohol (PVA) have had differing success at decontaminating surfaces with CWAs in reported studies. For example, Keisar *et al.* have demonstrated PVA/borate-based hydrogels that produce hydrogen peroxide and peracetic acid for remediating hydrophobic CWAs.[18] In their studies, their hydrogel formulations employed a co-solvent system of ethylene glycol and sodium dodecylbenzenesulfonate (SDBS) solubilizing hydrophobic CWAs. While the formulations were effective in oxidizing organophosphorus nerve agents like sarin, their performance with HD and CEES was less successful due to their incomplete miscibility with HD. The study observed a relatively long half-life of 1–2 h for HD and CEES captured within the hydrogel films, with complete oxidation requiring 10 h – significantly longer than the oxidation times (≤6 h) observed for other simulants in that study. Thus, to advance hydrogel-based remediation methods, challenges of improving both the miscibility of CWAs with water and the oxidizing capabilities of the formulations must be addressed.

Herein, we report our development of a PVA/borate-based hydrogel formulation that employs peroxymonocarbonate ions (HCO_4^-) and an amine oxide surfactant for accelerated degradation of CEES. Our strategy is twofold: (1) to increase the released amounts of reactive oxygen species (ROS) of high oxidizing power in the hydrogel as it forms, and (2) to achieve sufficient dissolution of CEES using an amine oxide surfactant without compromising the gelation process. Leveraging the common PVA/borate-based hydrogel formulation used by Keisar *et al.*,[18] our formulation incorporates a bicarbonate-activated peroxide (BAP) system[19] to generate HCO_4^- ions that are known for their strong oxidative capabilities[20] (Scheme 2). Aside from being highly oxidative at near-neutral pH,[21] as HCO_4^- ions react

with CEES, they re-generate bicarbonate ions, which can then cyclically produce more HCO_4^-, allowing for their long-term production.

To improve the homogeneous mixing of CEES within the hydrogel, we used the surfactant *N,N*-dimethyl-1-dodecylamine *N*-oxide (DDAO) instead of SDBS as in the study by Keisar *et al.*[18] due to the charge versatility of DDAO in various pH environments and hydrophilic headgroup.[22] In particular, DDAO is net neutral at neutral pH values and is not sterically hindered at its headgroup.[23] This allows for intermolecular forces between DDAO and CEES to solubilize CEES in aqueous environments without the production of new species or vesicles.[24] The efficiency of these two surfactants in solubilizing CEES was studied through DLS and ^1H NMR. Four hydrogel formulations were evaluated for their efficacy in oxidizing CEES. The production of HCO_4^- from NH_4HCO_3 and H_2O_2 was confirmed using both ^{13}C-NMR and Raman spectroscopy. The oxidation kinetics of CEES to its sulfoxide (CEESO) and sulfone (CEESOO) products were monitored *via* ^{13}C-NMR. Additionally, headspace gas chromatography-mass spectrometry (GC-MS) was employed to measure the airborne persistence of CEES above the hydrogel samples.

2 Experimental methods

2.1 Materials

Polyvinyl alcohol (PVA) with a molecular mass of 22 kDa was purchased from MP Biomedicals (Solon, OH, USA). Sodium tetraborate ($Na_2B_4O_7$), dodecylbenzenesulfonic acid, sodium salt (SDBS), deuterated oxide (D_2O), *para*-xylene (*p*-xylene), hydrogen peroxide (H_2O_2, 30% (w v^{-1}) solution), and ethylene glycol (EG) were acquired from Sigma Aldrich (Saint Louis, MO, USA). Tetraacetylethylenediamine (TAED), sodium tetraborate decahydrate ($Na_2B_4O_7 \cdot 10H_2O$), and sodium perborate monohydrate ($NaBO_3 \cdot H_2O$) were purchased from Thermo Scientific (Fair Lawn, NJ, USA). 2-Chloroethyl ethyl sulfide (CEES) and 2-(ethylthio)ethanol (HEES) were purchased from TCI (Portland, OR, USA), and methanol (MeOH) was purchased from VWR (Radnor, PA, USA). Ammonium bicarbonate (NH_4HCO_3) was purchased from Acros Organics (Antwerpen, Belgium). *N,N*-dimethyl-1-dodecylamine *N*-oxide (DDAO, 30% aqueous solution) was obtained from CHEM-IMPEX (Wood Dale, IL, USA). Nanopure water with 18.2 MΩ cm was obtained from a Synergy water purification system (VWR, Radnor, PA, USA) using lab-sourced deionized water.

2.2 Determination of peroxymonocarbonate ions as a function of H_2O_2 concentration

The concentrations of peroxymonocarbonate ion (HCO_4^-) in a range of hydrogel simulants composed of EG, NH_4HCO_3, and H_2O_2 were measured by Raman and ^{13}C-NMR spectroscopy. This simulant mixture was used because it allowed us to detect HCO_4^- by reducing any obstruction of signals from other chemicals or phase changes as in the hydrogel system. For an in-depth methodology of the Raman sample analysis and preparation, please see the SI.

$$HCO_3^- + H_2O_2 \rightleftharpoons HCO_4^- + H_2O$$
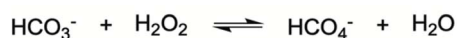
Scheme 2 Overall equilibrium reaction between bicarbonate ions and hydrogen peroxide leads to the production of peroxymonocarbonate ions.

A standardization calibration method was performed to determine the presence and concentration of HCO_4^- ions by ^{13}C-NMR in different mixtures of NH_4HCO_3, EG, and H_2O_2. Eight samples containing 7.5% (w v^{-1}) of NH_4HCO_3 and 15% (w v^{-1}) of EG with 0 to 8% (w v^{-1}) of H_2O_2 balanced in nanopure water were examined. The concentrations of H_2O_2 explored in these mixtures were 0, 1.5, 2, 3, 4, 5, 6, 7, and 8% (w v^{-1}). In a typical experiment, MeOH (20 μL), D_2O (50 μL), and the respective NH_4HCO_3–H_2O_2-EG solution (600 μL) were added to a 7″ 5 mm NMR tube. ^{13}C-NMR was run per sample using a Bruker Ascend 700 MHz NMR (Billerica, MA, USA) at 128 scans per experiment. A T_1 analysis was performed on the samples and resulted in a T_1 of about 2.5 s ^{13}C-NMR (700 MHz, D_2O), ppm: δ = 161.5, 159.5, and 49.8

2.3 Preparation of PVA-based hydrogel formulations

Four formulations of the PVA-based hydrogels composed of PVA, $Na_2B_4O_7$, EG, DDAO, TAED, $NaBO_3 \cdot H_2O$, NH_4HCO_3, and H_2O_2 (Formulations I, II, III, and IV) were evaluated in this study. These formulations differed from each other as they had different concentrations of NH_4HCO_3 (0 or 7.5% (w v^{-1})) and H_2O_2 (0 or 4% (w v^{-1})). The concentration of 4% (w v^{-1}) was chosen for H_2O_2 for safety and ease of transport to field applications. Each hydrogel was formed by mixing equal volumes (1 : 1 volume ratio) of two aqueous solutions, Solution A and Solution B, consisting of selected components in the chemical list. For example, to form a hydrogel of 2 mL in volume, Solution A (1 mL) was pipetted into a beaker, followed by pipetting Solution B (1 mL) into the pipetted Solution A. This method was used to observe the different gelation properties of the formulations on glass vials. Uniform gel formation typically occurred after swirling the mixture within a minute. The chemical compositions of Solution A and Solution B for these four formulations are listed in Table 1 (see SI for detailed preparation of these solutions).

2.3.1 Physical properties of PVA-based hydrogel formulations.
Photographs of the four formulated PVA-based hydrogels taken one hour after the mixing of Solutions A and B in a 1 : 1 ratio are presented in Fig. 1. These images feature the distinct physical characteristics and adherence properties of the four hydrogel formulations when applied to the surface of glass vials. Among these formulations, Formulation I exhibited the most significant presence of microbubbles within its matrix that contained the highest concentrations of oxidizing species (Fig. 1a). These microbubbles likely resulted from the reactions
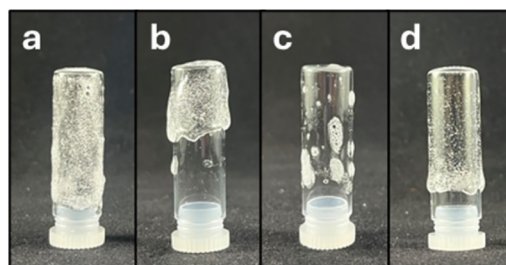

Fig. 1 Photos of the four formulated hydrogels: (a) Formulation I, (b) Formulation II, (c) Formulation III, and (d) Formulation IV. These photos were taken 1 hour after mixing the corresponding Solution A and Solution B in a 1 : 1 ratio.

between H_2O_2 and NH_4HCO_3, which produced HCO_4^- ions alongside gaseous byproducts such as CO_2. In comparison, Formulation II displayed increased viscosity, appearing "thicker" compared to the other formulations (Fig. 1b). While it produced less gel volume than Formulations I and IV, it maintained a cohesive structure (Fig. 1a and d). In contrast, Formulation III was markedly thinner and less viscous, with minimal microbubble formation (Fig. 1c). This formulation yielded the smallest volume of hydrogel, leaving most of the mixture in a liquid state (see Fig. S4). These observations highlight the variation in gelation and physical properties across the formulations, influenced by differences in the concentrations of reactive species and resultant gas formation.

2.4 Headspace characterization of half sulfur mustard gas by GC-MS

For GC-MS data acquisition, Solution A (150 μL) and MeOH (3 μL) were added to a glass vial, followed by the addition of Solution B (150 μL), *para*-xylene (3 μL as an internal standard), and CEES (2 μL) to the mixture. For proper gel formation, Solution B should be added in the middle of Solution A. This sample preparation process was performed for each formulation listed in Table 1. GC-MS was performed on a Thermo Scientific Trace 1310 Gas Chromatograph coupled with a Thermo Scientific ISQ LT Single Quadrupole Mass Spectrometer (Fair Lawn, NJ, USA). The GC-MS data were processed *via* the Chromeleon™ version 7.2.10 software (Fair Lawn, NJ, USA). Each clear vial had a holding capacity of about 2 mL and was capped using non-slit PTFE septa liner caps. Using an autosampler and a DB-5 column (column length: 30 m, inner

Table 1 Chemical compositions of Solution A and Solution B for the PVA-based hydrogel formulations: I, II, III, and IV

Formulation	Solution A			Solution B				
	PVA [%w v^{-1}]	TAED [%w v^{-1}]	NH_4HCO_3 [%w v^{-1}]	EG [%w v^{-1}]	DDAO [%w v^{-1}]	$Na_2B_4O_7$ [%w v^{-1}]	$NaBO_3 \cdot H_2O$ [%w v^{-1}]	H_2O_2 [%w v^{-1}]
I	5	0.05	7.5	15	5	2	2	4
II	5	0.05	7.5	15	5	2	2	0
III	5	0.05	0	15	5	2	2	4
IV	5	0.05	0	15	5	2	2	0

diameter: 0.320 mm, and film thickness: 0.50 μm), we followed the kinetics of the reaction for 10 experiments per sample. Each injection was 5 microliters from the headspace of the vial. This means that the injections were filled with gas in the vial above the hydrogel samples. The instrumental method ramped the temperature for the GC from 40 °C to 90 °C in 10 minutes, with a 1 minute hold time at 90 °C, a 10:5 split ratio, and scanned from 42 *m/z* to 160 *m/z*.

2.5 Characterization of oxidation kinetics of half-sulfur mustard gas

2.5.1 Preparation of NMR samples and acquisition of NMR data. To acquire NMR data for the oxidation kinetics analysis, Solution A (125 μL) and D_2O (25 μL) were added to a 4″ 3 mm NMR tube. CEES (2 μL) and MeOH (3 μL) were then added in succession to the NMR tube. MeOH was employed as an internal calibrant for both chemical shift and concentration. Afterward, Solution B (125 μL) was transferred to the NMR tube using a syringe to mix the two solutions. ^{13}C-NMR was run on each sample using 128 scans per experiment using a Bruker Ascend 700 MHz NMR. We followed the kinetics of this reaction by NMR for 30 experiments, which is about 3.25 h. This process was repeated for the four formulations studied. ^{13}C-NMR (700 MHz, D_2O) signals in ppm were monitored at δ = 161.5, 159.5, 49.8, 15.7, 15.3, 8.9, 6.8, 6.2. These carbon resonances were followed and integrated to determine the kinetic parameters. To calibrate the spectra, the locations of the ^{13}C peaks of MeOH were set at 49.8 ppm, with their integral areas set to 1. A full list of peaks observed and identified is provided in the SI (Table S1).

2.5.2 Software for data analysis. The NMR spectra were processed using the Bruker TopSpin 4.3.0 (Billerica, MA, USA). The percentage of oxidized CEES was computed using the ratio of the sum of the integral peak areas of singly oxidized CEES (CEESO) and doubly oxidized CEES (CEESOO) to the sum of the integral peak areas of CEES, CEESO, CEESOO, ethyl 2-hydroxyethyl sulfide (HEES), and ethyl(2-(ethylthio)ethyl)(2-hydroxyethyl)sulfonium chloride (HESC) in each measured ^{13}C-NMR spectrum, or ratio = $(A_{CEES} + A_{CEESO})/(A_{CEES} + A_{CEESO} + A_{CEESOO} + A_{HEES} + A_{HESC})$. The percentage of CEES hydrolyzed was likewise calculated using the ratio of the sum of the integral peak areas of HEES and HESC to the sum of the integral peak areas of all oxidized and hydrolyzed species, or ratio = $(A_{HEES} + A_{HESC})/(A_{CEES} + A_{CEESO} + A_{CEESOO} + A_{HEES} + A_{HESC})$.

2.6 Characterization of half-sulfur mustard in surfactant solutions

2.6.1 Size determination of micelles and vesicles by dynamic light scattering. The suspension of CEES in two different aqueous surfactant solutions was investigated by determining the size distributions of micelles and vesicles in these solutions before and after the addition of CEES. The particle sizing was achieved by analyzing 50 μL of the solution mixtures in a quartz cuvette by dynamic light scattering (DLS) on ZetaStar (Wyatt Technology, Goleta, CA, USA) with a scattering angle of 90.0° at 25 °C. The samples were shaken for 10 seconds before measurement to ensure that both suspended

and sedentary particles were sufficiently represented during the sizing process. 10 scans were performed in each measurement. The data was analyzed using the intensity-weighed multi-modal distribution model.

The two surfactants studied were SDBS and DDAO. The 5% (w v^{-1}) solution of SDBS was prepared in nanopure water, and its pH was adjusted to 8.4 using concentrated sodium hydroxide (NaOH). The 5% (w v^{-1}) solution of DDAO was similarly prepared, but its pH was adjusted to 8.6 instead. To evaluate the suspension of CEES, each CEES-surfactant solution mixture was prepared by combining 14.28 μL of CEES with 2 mL of the surfactant solution in a clear vial, followed by sonication for 10 minutes to homogenize the mixture. The DLS measurements were then performed at 24 min and 60 min after the sonication.

2.6.2 NMR analysis of half-sulfur mustard in surfactant solutions. The suspension of CEES in a 5% (w v^{-1}) SDBS surfactant solution and a 5% (w v^{-1}) DDAO surfactant solution was assessed using NMR analysis. Each NMR sample of the CEES-surfactant solution mixture was prepared by combining 2% (w v^{-1}) EG (4.5 μL), CEES (3 μL), D_2O (50 μL), and surfactant solution (445.5 μL) in a 5 mm NMR tube. Firstly, ^{1}H-NMR measurement for each sample mixture was performed using 8 scans per experiment on a Bruker 300 MHz NMR. The NMR sample was spun at 20 Hz, and the dissolution of CEES was tracked over 50 experiments, or across a period of about 50 min. The relative concentrations of the chemical components in solutions were monitored by examining the integral areas of peaks at 0.64 ppm (SDBS), 2.13 ppm (impurity in DDAO), 2.78 ppm (CEES), 2.97 ppm (HESC), 3.19 ppm (DDAO), 3.57 ppm (EG), and 3.63 ppm (HEES). Afterward, a ^{13}C-NMR measurement of the mixture was obtained with 1000 scans. ^{1}H-NMR (300 MHz, D_2O) ppm δ = 0.64 (3H, t, CH$_3$), 2.13 (impurity found in DDAO), 3.19 (2H, s, CH$_2$), 2.78 (2H, t, CH$_2$), 2.97 (2H, q, CH$_2$), 3.57 (4H, s, CH$_2$), and 3.63 (2H, t, CH$_2$). The formation of micelles could shift these peaks because of the matrix effect in the surfactant solutions.

3 Results and discussion

3.1 Production of peroxymonocarbonate ions

The formation of peroxymonocarbonate ions (HCO$_4^-$) from the reaction mixture of ammonium bicarbonate (NH$_4$HCO$_3$) and hydrogen peroxide (H$_2$O$_2$) in simulant gel solutions was verified using ^{13}C-NMR and Raman spectroscopy. The simulant gel solutions without PVA and DDAO were used instead, as they reduced the obstruction of ^{13}C signals due to phase changes during hydrogel formation and chemical byproducts from side reactions. In a typical ^{13}C-NMR spectrum of the gel simulant, the presence of HCO$_3^-$ and HCO$_4^-$ was represented by the peaks at 161 ppm and 159 ppm, respectively, consistent with literature reports[25] (Fig. 2a). Based on NMR measurements, a yield curve of HCO$_4^-$ ions was generated by varying the concentration of H$_2$O$_2$ from 0 to 8% (w v^{-1}) while keeping NH$_4$HCO$_3$ constant at 7.5% (w v^{-1}) in the simulant gels (Fig. 2b), showcasing the increase in the production of HCO$_4^-$ ions with an increase in the initial concentration of H$_2$O$_2$. The
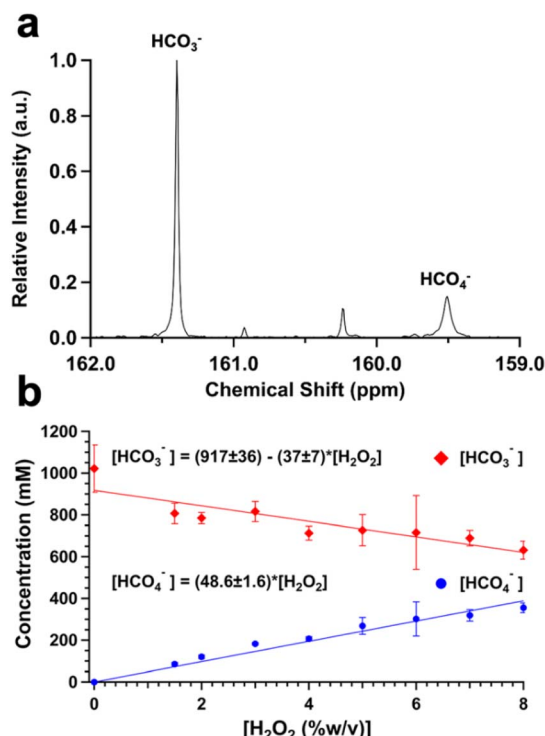
Fig. 2 ^{13}C-NMR study of the reaction between NH_4HCO_3 and H_2O_2. (a) ^{13}C-NMR spectrum showing the presence of peroxymonocarbonate ions (HCO_4^-) at 159.5 ppm and bicarbonate ions (HCO_3^-) at 161.5 ppm in an aqueous gel simulant mixture containing 7.5% (w v^{-1}) NH_4HCO_3, 15% (w v^{-1}) of ethylene glycol (EG), and 4% (w v^{-1}) H_2O_2. (b) Plot of the concentrations of HCO_4^- and HCO_3^- against the concentration of H_2O_2 in gel simulant mixtures comprised of 7.5% (w v^{-1}) NH_4HCO_3, 15% (w v^{-1}) of EG, and variable 0 to 8% (w v^{-1}) H_2O_2.

yield curve also shows that H_2O_2 is required for HCO_4^- formation, as NH_4HCO_3 alone does not produce detectable HCO_4^-.

Notably, as more H_2O_2 was added to the simulant gel formulations, the concentration of HCO_3^- decreased non-linearly. This behavior may result from pH effects on the equilibrium reaction producing HCO_4^- or from the conversion of HCO_3^- and other species, such as CO_2 and OH^-, observed in bicarbonate-activated peroxide (BAP) systems.[26] As another verification, we performed Raman spectroscopic studies of similar gel simulant mixtures comprising NH_4HCO_3, H_2O_2, EG, and calibrant $KClO_4$ (Fig. S1) to confirm the production of HCO_4^- ions. An analysis of the positive correlation in the production of HCO_4^- ions between Raman and NMR can be found in the SI (Fig. S2 and S3).

3.2 Oxidation kinetics of CEES by PVA-based hydrogels

The oxidation kinetics of CEES in four hydrogel formulations were evaluated by tracking the conversion of CEES to the oxidized products (CEESO and CEESOO) by NMR. Since CEES can be degraded through reaction pathways of hydrolysis and dehydrohalogenation, the presence of other hydrolyzed CEES byproducts was also monitored to determine the degradation progress of CEES in the hydrogels. The NMR measurements of hydrogel-CEES mixtures were collected over several time
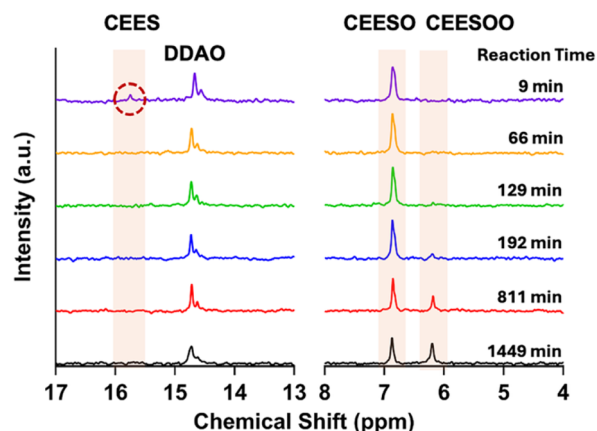

Fig. 3 ^{13}C-NMR spectra of the reaction between Formulation I PVA-based hydrogel and CEES over reaction time.

intervals: the initial measurement, hourly for the first 3 hours, at 12 hours, and at 24 hours. The identified ^{13}C peaks are displayed in Table S1.

Among the hydrogel formulations, Formulation I exhibited the fastest oxidation kinetics of CEES, followed by Formulation III, II, and IV. The ^{13}C-NMR spectra of Formulation I revealed the ^{13}C peaks of CEES at 15.7 ppm and CEESO at 6.8 ppm within the first 10 minutes of the reaction (Fig. 3). The ^{13}C peaks of the doubly oxidized CEES (CEESOO) at 6.2 ppm started to emerge after 129 minutes. During the examination period of 24 h, the integrated ^{13}C peak area of CEESO rose and decreased, while that of CEESOO continued to increase.

In contrast, the ^{13}C-NMR spectra of Formulation IV in the first 10 minutes showed the presence of two major products from the hydrolysis of CEES. They were HEES represented by a ^{13}C peak at 15.3 ppm, and ethyl(2-(ethylthio)ethyl)(2-hydroxyethyl) sulfonium chloride (hereafter referred to as HESC) represented by the ^{13}C peak at 8.9 ppm (Fig. S5). According to Bae *et al.*,[10] the hydrolysis of CEES may yield sulfonium salts as byproducts, such as HESC (Scheme 3). Thus,
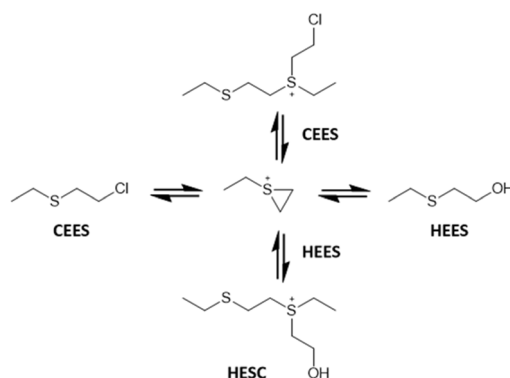
Scheme 3 Derivative products transformed from the treatment of CEES through hydrolysis. The chloride ion is omitted in the HESC structure. Reprinted (adapted) with permission from S. Y. Bae and M. D. Winemiller, *The Journal of Organic Chemistry*, 2013, **78**, 6457–6470. Copyright 2013 American Chemical Society.[10]
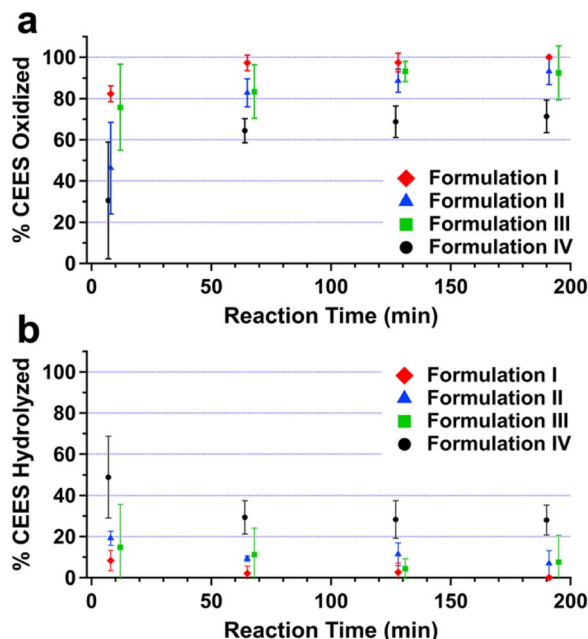
Fig. 4   (a) Percentages of oxidized CEES and (b) hydrolyzed CEES by PVA-based hydrogel Formulations I, II, III, and IV over 200 min.

the corresponding integrated peak areas were included in the calculations of the selectivity of reaction products from the hydrolysis and/or oxidation of CEES by hydrogels at different reaction times. For comparison, additional spectra of Formulation I with identified peaks from 0–70 ppm are provided in Fig. S6 of the SI.

The overall capabilities of the four hydrogel formulations to oxidize or hydrolyze CEES within 200 minutes in our experiments are summarized in Fig. 4 and 5. Formulation I demonstrated the most rapid and efficient degradation for CEES, achieving 97% CEES oxidation within 1 hour. Conversely, Formulations II, III, and IV could not reach that rate of degradation through oxidation. The most significant differences in

oxidation rates among the formulations were observed within the first 10 minutes, likely due to the higher concentrations of reactive oxygen species (ROS) produced in Formulation I. A comparison of the total percentage of CEES treated through either oxidation or hydrolysis revealed a high selectivity for oxidation from Formulation I, with only 8% of the total 90% CEES treated being hydrolyzed (Fig. 5). Probably due to their relatively lower levels of oxidants, these three formulations had a much higher degree of CEES hydrolysis at the beginning of the reactions (Fig. 5). Nonetheless, after 24 hours of reaction, all formulations could achieve an oxidation rate of 75 + % of CEES (Fig. S7 in SI). For clarity, the numerical values underlying the trends shown in Fig. 5 are summarized in Table S2.

The superior degradation efficiency of Formulation I over the other three formulations was attributed to its elevated concentrations of oxidizing species and the production of highly reactive HCO_4^- ions from the BAP system in the hydrogel. The reactions underlying CEES oxidation in the examined hydrogels are summarized in Scheme 4. The inclusion of the NH_4HCO_3–H_2O_2 system in Formulation I significantly enhanced the reactive oxygen species (ROS) production through reaction eqn (2)–(4). Eqn (2) shows the general reaction for the generation of HCO_4^- ions, which possess a longer lifespan and stronger oxidizing power than PAA (Scheme 4). We hypothesize that this BAP system follows a similar mechanism for the formation of HCO_4^- ions elucidated by Zhao et al.[25] shown in the SI. Additionally, HCO_4^- ions can oxidize CEES to CEESO while producing bicarbonate ions (HCO_3^-), which further drive the equilibrium of eqn (3) forward to generate more HCO_4^- ions. Combined with PAA and additional ROS from H_2O_2 in Formulation I, the inclusion of HCO_4^- substantially increased the oxidation rate, which then promoted the selectivity of the CEES degradation pathway towards oxidation over hydrolysis. This was indirectly reflected by the lack of notable concentrations of hydrolyzed CEES products (HEES and HESC) in the mixture of Formulation I and CEES at the beginning of the CEES degradation process. Since the four formulations were inspired by the PVA-based hydrogel study by Keisar et al.,[18] they all utilized TAED and sodium perborate monohydrate to generate peracetic
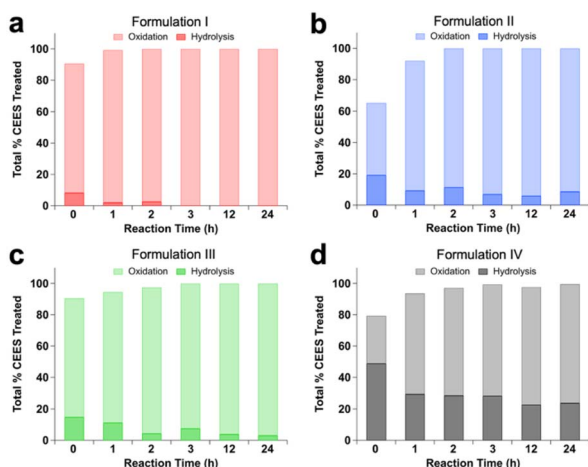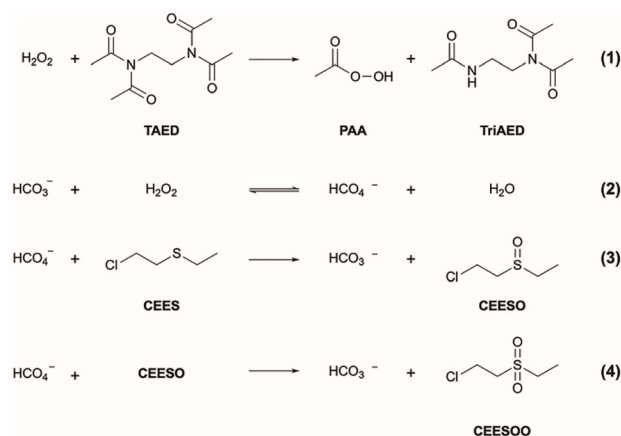

Fig. 5   Total percentage of CEES treated through both oxidation and hydrolysis for Formulations (a) I, (b) II, (c) III, and (d) IV at ca. 0, 1, 2, 3, 12, and 24 h.

Scheme 4   Reactions leading to the production of peracetic acid (PAA) and HCO_4^-, the primary oxidizing agents that oxidize CEES.

acid (PAA) as an independent but minor oxidant for CEES (eqn (1)). The presence of H_2O_2 in Formulation IV through sodium perborate hydrolysis is discussed in the SI (Scheme S2).

3.3 Roles of surfactants in enhancing the oxidation kinetics of CEES by PVA-based hydrogels

The surfactants in the PVA-based hydrogel formulations played a significant role in solubilizing CEES and enhancing their oxidation kinetics. Since the hydrophobic nature of CEES leads to its low solubility in aqueous environments, it is essential to promote its dissolution in the hydrophilic hydrogels for efficient degradation. As EG is not adequate to fully dissolve the CEES in the hydrogel, a co-solvent system using a surfactant was implemented.[18] DDAO is an amphoteric surfactant and is nonionic in the high pH media in our hydrogel study. To determine its effectiveness in suspending CEES, we studied a mixture of CEES with 5% (w v^{-1}) DDAO and a lower concentration of EG to reduce its oversaturation of the signal using ^{13}C-NMR. Aside from being a dissolution promoter, EG also served as an internal calibrant to indicate the relative concentrations of solubilized CEES and degraded byproducts. The ^{1}H and ^{13}C-NMR spectra of CEES added to an aqueous mixture of DDAO and EG revealed the hydrolysis of CEES to HEES and HESC (Fig. S8 and S9 in the SI). Within 10 minutes of chemical mixing in the NMR sample, the relative concentration of CEES increased and reached a plateau before its degradation decreased, suggesting the full incorporation of CEES into the mixture (Fig. 6).

Our kinetics studies showed a 92% decrease in the concentration of CEES in the NMR sample mixture of CEES, DDAO, and EG within an hour through hydrolysis. Based on the findings of Bae *et al.*, the production of HESC was favoured as HEES was formed from the hydrolysis of CEES[10] (see Scheme 3). As HEES was a stronger nucleophile than water, it could react with the cyclic sulfide intermediate to form HESC. This transformation rationalized the drop in the concentration of HEES

over time. Since the production of these sulfonium salt byproducts followed reversible pathways, their concentrations were expected to vary over time. Such trends were confirmed by tracing the ^{13}C-NMR peaks in spectra of HEES and HESC at chemical shifts consistent with those of the literature[10] (Fig. S9 in SI).

The effect of DDAO on accelerating the dissolution and degradation of CEES can also be corroborated by the evolution of the size distribution of micelles and/or vesicles in the aqueous mixture of CEES with DDAO and EG (Fig. 7). Right after mixing these components, the CEES initially formed a layer at the bottom of the mixture, and the particle sizing of the mixture only indicated the presence of DDAO micelles of 3–8 nm (Fig. 7a). After 24 min, the mixture turned turbid and the distribution of major particle sizes (or diameters) was bimodal, suggesting the presence of micelles of 2–11 nm and vesicles of 100–1000 nm in size. After an hour, the mixture became clear, but the size distribution of the particles in it remained similar. The phenomenological transition in the turbidity of the mixture revealed the active dissolution of CEES by the surfactant. Possibly owing to its amphoteric nature, DDAO might have facilitated the formation of positively charged CEES intermediates in their reversible hydrolysis reactions (see Scheme 3), which might in turn promote the dissolution of CEES. Notably, our similar investigation of the anionic surfactant SDBS showed the weak capability of SDBS to promote the dissolution and degradation of CEES within 1 hour (see Fig. S10–S14 in the SI). Since the hydrogel by Keisar *et al.*[18] that inspired our study
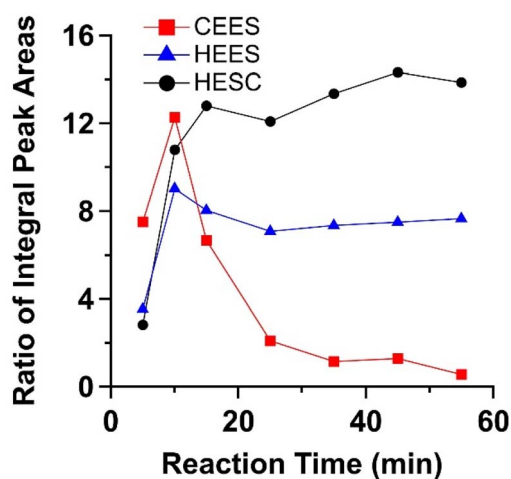

Fig. 6 Ratios of ^{1}H-NMR integral peak areas of CEES, HEES, and HESC to that of EG in an aqueous mixture of CEES in 5% (w v^{-1}) DDAO with 2% (w v^{-1}) EG over time.
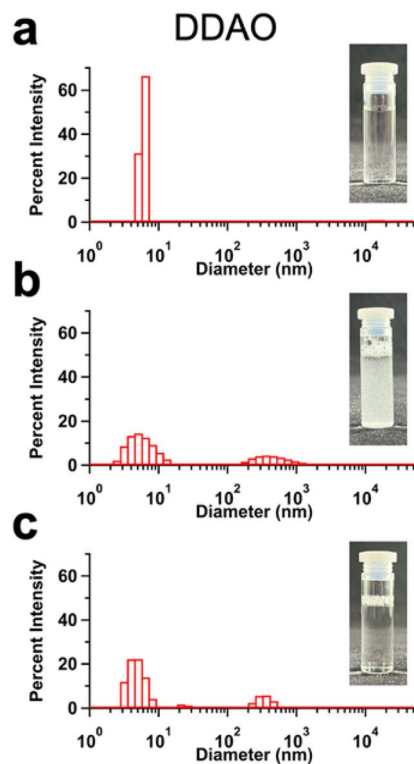

Fig. 7 DLS measurements of 5% (w v^{-1}) DDAO with the addition of CEES after (a) 0 min, (b) 24 min, and (c) 60 min. (Insets) Photos of mixtures.

employed SDBS in its formulation, the lower effectiveness of SDBS might partially explain why such hydrogels required 12+ hours to achieve substantial CEES degradation in that study.

3.4 Determination of CEES released from PVA-based hydrogels by headspace GC-MS

The release of CEES vapor from mixtures of CEES and the four formulations of hydrogels during the degradation process was traced and studied using headspace GC-MS analysis. *Para*-xylene (*p*-xylene) was used as an internal standard in the mixtures because of its high vapor pressure. The initial head-space GC-MS chromatograms showed three peaks (Fig. 8), with corresponding mass spectra representing *p*-xylene, CEES, and hydroxyethyl ethyl sulfoxide (HEESO) (Fig. S15 in the SI).

The plot of relative peak areas of CEES normalized by the peak area of the calibrant *p*-xylene from the chromatograms is illustrated in Fig. 9. The plot showed that the relative concentration of CEES to that of the calibrant in the vapor above the CEES-hydrogel mixtures decreased by 94–98% within the first 90 minutes of the reaction. These decreases further dropped to 99–100% after 120 minutes. The decreasing trends for mixtures with each formulation also indirectly illustrated that Formulations I, II, and III were more effective in oxidizing CEES than Formulation IV, reflecting the observed trends from the NMR analysis.

3.5 Comparisons of recent advances in the remediation of CEES

The hydrogel developed in this study has three major advantages over other recently published remediation methods for CEES reviewed in Table S3 in the SI. First, the use of HCO_4^-
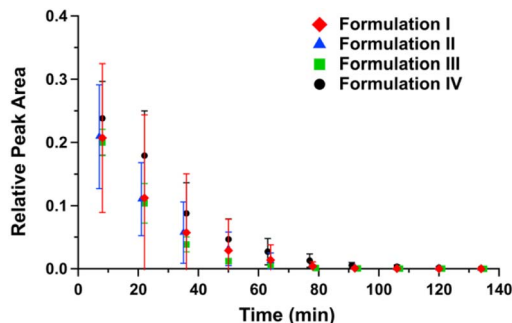

Fig. 9 Headspace GC-MS quantification of CEES in the vapor above four differently formulated PVA-based hydrogels with CEES over time. Plot of relative peak area of CEES normalized by the peak area of the calibrant *para*-xylene from GC-MS chromatograms over time.

drastically increased the selectivity for oxidation in Formulation I. As shown in Scheme 4, hydrolysis not only produces multiple byproducts, but HESC can also revert to CEES. Second, our current hydrogel system is compatible with the remediation of hydrophobic CEES in aqueous media with a DRE of up to 90% in 10 min. Except for the catalyst system of molybdate-based polyoxometalates, the rest of the reported catalysts in Table S3 required flammable, polar organic solvents or highly acidic media to achieve high CEES degradation efficiency. We were able to circumvent the need for non-polar solvents by using an adequate surfactant like DDAO to facilitate the dissolution of CEES in water. Since our solvent is water, the use of our hydrogel is more versatile than the cases that need non-polar solvents.

In addition, our developed hydrogel is less toxic than the materials in the previous remediation methods in Table S3 because it does not employ heavy metals in its formulation. The major chemicals in the hydrogel include biomedical-grade PVA and sodium tetraborate, in which boron has been shown as a necessary mineral nutrient for plant growth.[27] Additionally, DDAO in our formulation is a widely used surfactant due to its antimicrobial properties[28] and is used in detergents and cosmetics.[29] The BAP system uses H_2O_2 and NH_4HCO_3. H_2O_2 has been used to treat a variety of substances such as pesticides, dyes, and pharmaceuticals.[30] As a strong oxidizing agent, H_2O_2 is commonly studied and used in advanced oxidizing processes for the decontamination of wastewater.[31] The common decomposition products of H_2O_2 are water and oxygen. NH_4HCO_3 is typically used due to its pH regulatory properties[32] and has even been used in food as a leavening agent.[33] Note that the toxicity of HD and its oxidation products was studied by Wagner *et al.* The study found that the doubly oxidized species (HDO_2) is more toxic than HD and the singly oxidized sulfoxide (HDO).[34] Similarly, the toxicity of the singly oxidized CEES (CEESO) has been shown to be lower than that of the starting material, CEES, and the doubly oxidized CEES (CEESOO).[35] Overall, our hydrogel formation offers less toxic residual chemicals than CEES and is less harmful to the environment than the chemicals in the aforementioned methods in Table S3.
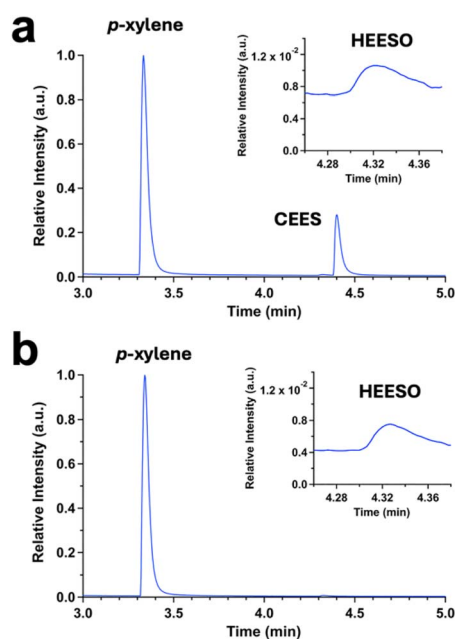

Fig. 8 Headspace gas-mass spectrometry chromatograms of Formulation I PVA-based hydrogel with CEES at reaction times of (a) 7 minutes and (b) 64 minutes.

4 Conclusions

In this study, we demonstrated the combined use of a bicarbonate-activated peroxide (BAP) system, specifically NH_4HCO_3–H_2O_2, and an amine oxide surfactant in a PVA-based hydrogel formulation to accelerate the oxidative degradation kinetics of CEES captured by the hydrogel. The HCO_4^- ions from the reversible reaction between NH_4HCO_3 and H_2O_2 were found to increase the oxidative capability of the hydrogel. The co-solvent system of the amine-oxide surfactant, DDAO, and ethylene glycol was verified to greatly increase the solubility of CEES in the hydrogel, facilitating the rapid oxidation of this compound. Among our four evaluated hydrogel formulations, our best formulation, Formulation I containing both the NH_4HCO_3–H_2O_2 system and DDAO, was observed to achieve a DRE of >99% within 60–80 min, superseding the oxidative kinetics of CEES by the hydrogel developed by Keisar et al.[18] Through headspace GC-MS analysis, we illustrated the capability of our developed hydrogel to capture volatile CEES and convert it to its oxidized products. This work is expected to stimulate future research in utilizing the NH_4HCO_3–H_2O_2 system with other hydrogels for applications that require sustained delivery of powerful oxidizers. Additionally, studies on the oxidative kinetics of common nerve agent simulants may be pursued as they are anticipated to accelerate under the improved conditions of the reported hydrogel formulation.

Author contributions

De Leon: data curation (lead); formal analysis (lead); investigation (lead); visualization (equal); writing – original draft (equal); writing – reviewing and editing (equal). Anderson: data curation (supporting); investigation (supporting). Maruyama: data curation (supporting); investigation (supporting). Darveau: conceptualization (equal); data curation (supporting); formal analysis (supporting); investigation (supporting); supervision (equal); writing – original draft (equal). Van Buren: conceptualization (equal); funding acquisition (equal); project administration (equal). Morton: conceptualization (equal); formal analysis (supporting); funding acquisition (equal); supervision (equal); writing – review and editing (equal). Cheung: conceptualization (equal); formal analysis (supporting); funding acquisition (equal); supervision (equal); visualization (equal); writing – original draft (equal); writing – reviewing and editing (equal).

Conflicts of interest

There are no conflicts to declare.

Data availability

The data supporting, including numerical data for all displayed figures, are available at Figshare at **https://doi.org/10.6084/m9.figshare.c.7902548**.

Supplementary information: Raman, NMR, and DLS data of PVA-hydrogels and controls; preparation of gel solutions; experimental data; expanded discussion on the identification of peroxymonocarbonate ions and the mechanisms for the formation of oxidizing species. See DOI: **https://doi.org/10.1039/d5ra05341b**.

References

1 B. Ma, G. Zuo, B. Dong, S. Gao, L. You and X. Wang, *New J. Chem.*, 2021, **45**, 20569–20574.
2 Y. C. Hudiono, A. L. Miller, P. W. Gibson, A. L. Lafrate, R. D. Noble and D. L. Gin, *Ind. Eng. Chem. Res.*, 2012, **51**, 7453–7456.
3 L. A. Power, P. J. M. Sessink, K. Gesy and F. Charbonneau, *Hosp. Pharm.*, 2014, **49**, 355–362.
4 U. S. Centers for Disease Control and Prevention, Mustard Gas in Chemical Emergencies, **https://www.cdc.gov/chemical-emergencies/chemical-fact-sheets/mustard-gas.html**, accessed 06/13/2025.
5 U. S. Centers for Disease Control and Prevention, Methods Used to Destroy Chemical Warfare Agents, **https://archive.cdc.gov/www_cdc_gov/nceh/demil/methods.htm**, accessed 06/13/2025.
6 D. Vergun, DOD Approaches Goal of Destroying All Stockpiled Chemical Weapons, **https://www.defense.gov/News/News-Stories/Article/Article/2354786/dod-approaches-goal-of-destroying-all-stockpiled-chemical-weapons/**, accessed 06/13/2025.
7 N. Emmanuel, P. Bianchi, J. Legros and J.-C. M. Monbaliu, *Green Chem.*, 2020, **22**, 4105–4115.
8 C. Weetman, S. Notman and P. L. Arnold, *Dalton Trans.*, 2018, **47**, 2568–2574.
9 D. Li, W. Wu, H. Zhang, C. Cheng, B. Zhuang, B. Zhang, H. Wu and Y. Xiao, *J. Mol. Liq.*, 2023, **385**, 122407.
10 S. Y. Bae and M. D. Winemiller, *J. Org. Chem.*, 2013, **78**, 6457–6470.
11 S. L. Giles, A. Sousa-Castillo, E. Y. Santiago, A. P. Purdy, M. A. Correa-Duarte, A. O. Govorov and O. A. Baturina, *Colloid Interface Sci. Commun.*, 2021, **41**, 100362.
12 E. Mahayoni, S. Min, J. Kim, K. Jeong and S. H. Kim, *J. Hazard. Mater.*, 2021, **411**, 125144.
13 M. Florent, D. A. Giannakoudakis and T. J. Bandosz, *Langmuir*, 2017, **33**, 11475–11483.
14 L. Liu, K.-A. Min, M. Tayyab, B. Han and C.-H. Lee, *Environ. Adv.*, 2022, **9**, 100255.
15 M. Sadeghi, H. Ghaedi, S. Yekta and E. Babanezhad, *J. Environ. Chem. Eng.*, 2016, **4**, 2990–3000.

16 J. Yin, C. Huang, Y. Zhou, L. Zhang, N. Li and R. Sun, *Ind. Eng. Chem. Res.*, 2022, **61**, 7699–7708.

17 E. M. Ahmed, *J. Adv. Res.*, 2015, **6**, 105–121.

18 O. Redy Keisar, V. Nahum, L. Yehezkel, I. Marcovitch, I. Columbus, G. Fridkin and R. Chen, *ACS Omega*, 2021, **6**, 5359–5367.

19 X. Yang, Y. Duan, J. Wang, H. Wang, H. Liu and D. L. Sedlak, *Environ. Sci. Technol. Lett.*, 2019, **6**, 781–786.

20 E. Linares, D. Severino, D. R. Truzzi, N. Rios, R. Radi and O. Augusto, *Chem. Res. Toxicol.*, 2024, **37**, 1129–1138.

21 A. Jawad, Z. Chen and G. Yin, *Chin. J. Catal.*, 2016, **37**, 810–825.

22 R. A. Abdel-Rahem, *J. Chem. Eng. Data*, 2012, **57**, 957–966.

23 V. Lair, S. Bouguerra, M. Turmine and P. Letellier, *Langmuir*, 2004, **20**, 8490–8495.

24 K. D. Thompson, E. P. Danielson, K. N. Peterson, N. O. Nocevski, J. T. Boock and J. A. Berberich, *Langmuir*, 2022, **38**, 4090–4101.

25 S. Zhao, H. Xi, Y. Zuo, Q. Wang, Z. Wang and Z. Yan, *J. Hazard. Mater.*, 2018, **344**, 136–145.

26 H. Pan, Y. Gao, N. Li, Y. Zhou, Q. Lin and J. Jiang, *Chem. Eng. J.*, 2021, **408**, 127332.

27 S. Li, L. Yan, M. Venuste, F. Xu, L. Shi, P. J. White, X. Wang and G. Ding, *Chemosphere*, 2023, **338**, 139474.

28 C. R. Birnie, D. Malamud and R. L. Schnaare, *Antimicrob. Agents Chemother.*, 2000, **44**, 2514–2517.

29 M. Baglioni, Y. Jàidar Benavides, D. Berti, R. Giorgi, U. Keiderling and P. Baglioni, *J. Colloid Interface Sci.*, 2015, **440**, 204–210.

30 R. Li, D. Speed, D. Siriwardena, S. Fernando, S. M. Thagard and T. M. Holsen, *Chem. Eng. J.*, 2021, **425**, 131785.

31 C. Weng, Y.-H. Chuang, B. Davey and W. A. Mitch, *Environ. Sci. Technol.*, 2020, **54**, 12593–12601.

32 E. Honarvar and A. R. Venter, *J. Am. Soc. Mass Spectrom.*, 2017, **28**, 1109–1117.

33 R. G. M. van der Sman, *Curr. Res. Food Sci.*, 2021, **4**, 191–199.

34 G. W. Wagner and Y.-C. Yang, *Ind. Eng. Chem. Res.*, 2002, **41**, 1925–1928.

35 Y. Liu, C. T. Buru, A. J. Howarth, J. J. Mahle, J. H. Buchanan, J. B. Decoste, J. T. Hupp and O. K. Farha, *J. Mater. Chem. A*, 2016, **4**, 13809–13813.